doi:10.1017/S1431927622006882
Microsc. Microanal. 28 (Suppl 1), 2022

In-situ Imaging of Thermally Activated Atomic Reconstruction of Twisted Bilayer Transition Metal Dichalcogenides

Yichao Zhang[1], Chia-Hao Lee[1], Gillian Nolan[1], Ji-Hwan Baek[2], Gwan-Hyoung Lee[2], and Pinshane Y. Huang[1]

[1.] Department of Materials Science and Engineering, University of Illinois Urbana-Champaign, Urbana, IL, United States.
[2.] Department of Materials Science and Engineering, Seoul National University, Seoul, Korea.
* Corresponding author: pyhuang@illinois.edu

Moiré superlattices in twisted two-dimensional (2D) materials have drawn major research interest because of their ability to host a variety of emergent quantum phenomena, including unconventional superconductivity [1], quantum anomalous Hall effect [2], and ferroelectricity [3]. These phenomena are highly sensitive to twist angle, a degree of freedom unique to 2D interfaces that can be used to modulate periodic potential of the resulting moiré. Beyond pre-determined twist angles with tear-and-stack techniques, post-annealing [4] and spontaneous [5] rotations of twisted crystals have been reported, adding further complexity to precise control of twist angle. Therefore, exploring the thermal stability of twist angles of the moiré superlattice is crucial to reliable measurements of angle-sensitive quantum systems. However, *in situ* characterization of thermally induced, atomic-scale structural evolution in 2D material systems is challenging due to their high susceptibility to electron-beam damage, especially at elevated temperature. In our work, we discover a new atomistic mechanism of local reconstruction from moiré pattern to parallel (3R) and/or antiparallel (2H) domains in twisted bilayer 2D transition metal dichalcogenides (TMDCs). Unlike previous reports, where the twist angle is altered by the rotation of a whole flake, we observe the nucleation and growth of commensurate domains through the addition of grain boundaries.

Here, we report thermally activated, local reconstruction of twisted bilayer TMDCs using *in situ* aberration-corrected scanning transmission electron microscopy (STEM) and dark-field transmission electron microscopy (DFTEM). We fabricate graphene encapsulated twisted WSe_2 homo-bilayers and $MoSe_2$-WSe_2 hetero-bilayers positioned on MEMS-based chips for *in situ* pulsed heating (Figure 1a,b). Graphene encapsulation can mitigate electron-beam damage while being highly electron transparent. Instead of whole-flake rotation, we show that heat-pulses induce *local* reconstruction to parallel/antiparallel structures (referred to as aligned structures) ranging from a few nanometers to micrometers in size. Such reconstruction is observed in all samples exhibiting five different twist angles. *In situ* aberration-corrected annular dark-field (ADF) STEM imaging reveals that the aligned structure is formed by the nucleation of a new grain within one layer, surrounded by grain boundaries formed by 5|7 ring defects (Figure 1d,e) that enables the local, collective rotation of atoms. To capture the dynamic process of nucleation and growth of the aligned structure, we obtain a pair of complimentary DFTEM images after each applied heat pulse using one Bragg spot from each lattice separately (Figure 2a). In this way, intensity gain in one image and loss in the other image indicates local rotation and formation of a new aligned structure. Using this method, we observe nucleation of aligned structures between 200-1000°C (Figure 2b,c). The migration of the aligned-moiré interface scales linearly with respect to temperature (Figure 2d), unlike previously reported immobility of 5|7 grain boundaries [6]. These results provide new insights into the mechanisms of interlayer rotation at the atomic scale and potential method into engineering the structure of moiré superlattices.

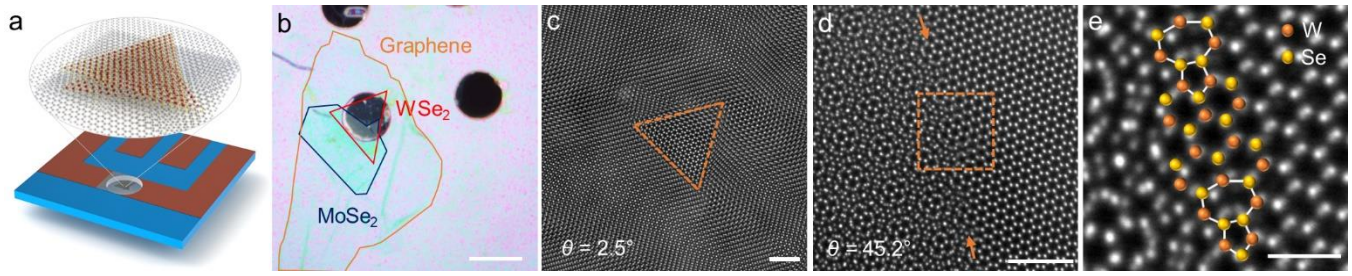

Figure 1. Local reconstruction from moiré superlattice in twisted bilayer TMDCs. **a**, Schematic of graphene encapsulated twisted bilayer TMDCs on a MEMS-based heating chip. **b**, Optical image of graphene encapsulated twisted $MoSe_2$-WSe_2 hetero-bilayer. Scale bar = 10 μm **c**, Fourier filtered ADF-STEM image of triangular-shaped (orange) antiparallel region in twisted WSe_2 homo-bilayer (twist angle = 2.5°). Scale bar = 2 nm for **c**,**d**. **d**, Fourier filtered ADF-STEM image of antiparallel-moiré interface marked with orange arrows in twisted $MoSe_2$-WSe_2 hetero-bilayer (twist angle = 45.2°). Dashed orange box marks position of panel **e**. **e**, Magnified Fourier filtered ADF-STEM image overlaid with 5|7 ring defects at the antiparallel-moiré interface labeled in **d**. Scale bar = 1 nm. Twist angle is defined as 0° for parallel alignment and 60° for antiparallel alignment.

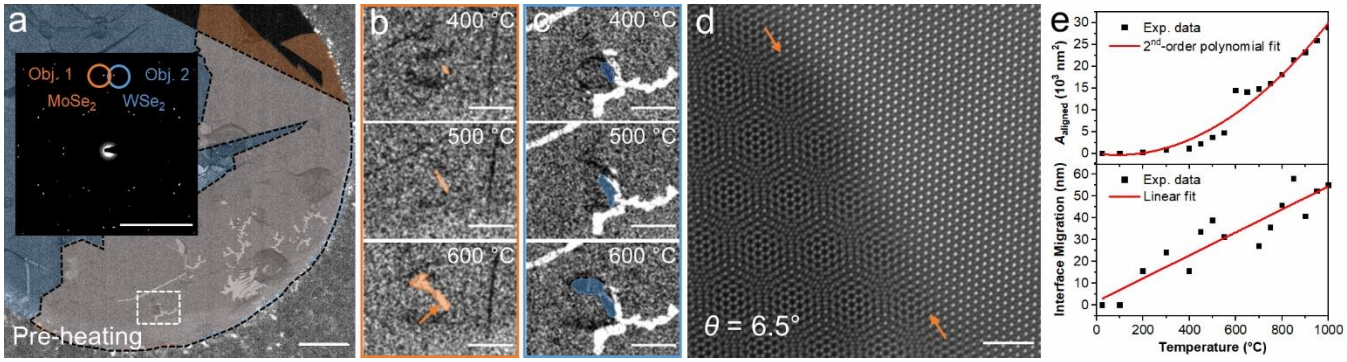

Figure 2. Growth of parallel-aligned structure in a twisted $MoSe_2$-WSe_2 hetero-bilayer. **a**, Composite DFTEM image of $MoSe_2$ (orange) and WSe_2 (blue) before applying heat pulses. Dashed black polygon marks the position of the twisted bilayer region. Dashed white rectangle marks region of interest (ROI) in **b**,**c**. Scale bar = 1 μm. Inset is selected-area electron diffraction pattern of twisted $MoSe_2$-WSe_2 hetero-bilayer. Colored circles mark positions of objective apertures 1 and 2 used to generate DFTEM images of $MoSe_2$ (orange) and WSe_2 (blue) layers separately in **a**-**c**. Scale bar = 5 nm^{-1}. **b**,**c**, Select DFTEM images of ROI obtained with objective apertures 1 and 2, respectively, at 400 °C, 500 °C, and 600 °C. Orange and blue polygons mark regions gaining and losing intensity, respectively. Orange arrow marks position where **d** was obtained. Scale bar = 500 nm. **d**, Fourier filtered ADF-STEM image of parallel-moiré interface marked with orange arrows in twisted $MoSe_2$-WSe_2 hetero-bilayer (twist angle = 6.5°). **e**, Temperature-dependent growth of aligned structure. Area of aligned structure (top panel) exhibits polynomial dependence on temperature. Migration of interface (bottom panel) per heat pulse displays linear dependence on temperature.

References:

[1] Y Cao, et al., Nature, **556** (2018), p. 43.
[2] M Serlin, et al., Science, **367** (2020), p. 900.
[3] L Li, M Wu, ACS Nano, **11** (2017), p. 6382.
[4] L Wang, et al., Science, **350** (2015), p. 1231.

https://doi.org/10.1017/S1431927622006882 Published online by Cambridge University Press

[5] S Zhu, P Pochet, HT Johnson, ACS Nano, **13** (2019), p. 6925.
[6] X Liu, et al., Nanoscale, **12** (2020), p.17746.

[7]The authors acknowledge funding support from the Department of Energy under award number DE-SC0020190. This work was carried out in part in Materials Research Laboratory at UIUC.

https://doi.org/10.1017/S1431927622006882 Published online by Cambridge University Press